Hindawi
Adsorption Science & Technology
Volume 2023, Article ID 8348431, 13 pages
https://doi.org/10.1155/2023/8348431

Research Article

Mesoscopic Process Simulation of In Situ Leaching of Ionic Rare Earth Based on NMRI Technology

Fuyu Wu,[1] **Dan Wang**,[2] **Yunzhang Rao**,[1,2] **Meidao Zhang**,[2] **Liang Shi**,[1,2] **Min Han**,[2] **and Wei Xu**[2,3]

[1]*School of Civil and Surveying & Mapping Engineering, Jiangxi University of Science and Technology, Ganzhou 341000, China*
[2]*School of Resources and Architectural Engineering, Jiangxi University of Science and Technology, Ganzhou 341000, China*
[3]*The Seventh Geological Brigade of Jiangxi Bureau of Geology, Ganzhou 341000, China*

Correspondence should be addressed to Yunzhang Rao; raoyunzhang@jxust.edu.cn

Received 31 August 2022; Revised 18 October 2022; Accepted 25 November 2022; Published 8 March 2023

Academic Editor: Juan A. Cecilia

In order to simulate and calculate the leaching process of ionic rare earths more realistically, a digital model of ionic rare earths with real size, shape, seepage channel, and pore ratio and distribution at the mesoscopic scale was constructed based on nuclear magnetic resonance imaging (NMRI) technology. And the in situ leaching mining process was simulated and calculated by using three control equations of solution seepage, ion exchange, and solute migration. The reliability of the NMRI model was verified by the results of the indoor column leaching experiment, and the influence of the injection intensity and leaching agent concentration on the leaching of rare earth ions was analyzed. The results show that there are dominant seepage channels in the ore body, and the rare earth ion exchange reaction and migration in the dominant channel area are completed first. By analyzing the leaching results of rare earth ions under the working conditions of different injection strengths and different concentrations of leaching agent, the results show that the injection strength and the concentration of leaching agent have an obvious promoting effect on the leaching of rare earth ions in a certain range. The injection strength of 0.5~1.0 mL/min and the concentration of 0.20~0.25 mol/L leaching agent are considered to be more economical in practical engineering.

1. Introduction

Ion-adsorbed rare earth minerals are mainly distributed in the south of China and are named for rare earth elements adsorbed in the form of cations on the surface of clay minerals weathered by granite or volcanic rocks. They are unique and important rare earth minerals in China [1, 2]. Rare earth cations adsorbed on the surface of clay minerals undergo ion exchange reaction in strong electrolyte solution and enter the solution [3]. Based on this characteristic, in situ leaching technology is developed to mine such rare earth minerals [4, 5]. In the actual promotion and application process of this technology, key issues such as leaching cycle, leaching rare earth concentration, and leaching efficiency have always been the focus of technical personnel and scientific researchers in the industry [6–8].

At present, many researchers describe the leaching process by establishing numerical models [9–11] and study the leaching process and mechanism by means of numerical simulation. Sheikhzadeh et al. [12] established an unsteady two-dimensional model of the unsaturated flow of the liquid in the uniform spherical ore bed based on the mass conservation equation of the liquid phase in the ore bed and the particles and solved the model with the full implicit finite difference method and obtained the influence of the periodic permeability of water on the saturation and vertical velocity distribution in the ore body. Liu et al. [13] established the governing equation for the elastic deformation seepage of ore and the governing equation for mass transfer, solved the two governing equations through porosity coupling, and simulated the change law of the concentration of leaching agent and leaching ion in constant head leaching. Hu et al. [14] used Kerr model, Vanselow model, and Gapon

model to describe the solid-phase rare earth ion exchange process; analyzed the error between the calculated value and the test value under those three models; and proposed the suggestion of using Kerr model to describe the solid-phase rare earth ion exchange process. Long et al. [15] used the convective dispersion equation to describe the solute transport process in the one-dimensional column leaching test of ionic rare earth and analyzed the influence of different concentrations of leaching agents on the leaching rate of rare earth. Wu et al. [16, 17] established a fully coupled flow-reaction-deformation-mass transfer model in the leaching process on the basis of the original results, considering the deformation factors of ore in the leaching process, and studied the distribution of porosity, saturation, leaching agent concentration, and leached ore concentration in the ore pile under the condition of one-dimensional fixed spray and fixed water head. Based on the mass conservation of fluid and solute, combined with the influence of consolidation effect on soil mass, Tan [18] established a coupled numerical model of seepage-reaction-stress of ionic type rare earth in situ leaching and studied the distribution and space-time evolution of seepage field, stress field, and concentration field under different injection pressure, axial pressure, and confining pressure factors during column leaching, respectively.

Most of the previous studies treated ore bodies as homogeneous porous media without considering the influence of the nonuniformity of particle size and the disorder of particle distribution on the seepage flow of rare earth ore bodies [19–21]. With the development of testing technology, more and more researchers try to use NMRI, CT, and other technologies to study the internal pore structure of ore bodies. Ma et al. [22, 23] used CT technology to collect pore images of ore and rock granular media and found that the porosity of ore and rock media in heap leaching system had spatial and temporal variability. Li et al. [24] established the ore body pore model of different layers of ion-type rare earth ore through CT scanning technology and analyzed the influence of ion-type rare earth cavity process on the ore body pore network. Yang et al. [25] explored the microstructure change rule of ion-type rare earth ore body during leaching by NMRI technology and analyzed the influence of leaching agent pH on the leaching rule of ion-type rare earth.

In order to reflect the real seepage channel and the process of complex ion exchange and migration in the rare earth ore body, this paper constructed the seepage channel in rare earth ore body by NMRI technology and established a numerical model of seepage-exchange-migration in situ leaching of ionic rare earth on the basis of Navier-Stokes equation, exchange reaction equation, and convection-diffusion equation. COMSOL Multiphysics multiphysical field coupling software was used to study the seepage-exchange-migration evolution law in the leaching process under different injection strengths and leaching agent concentrations and analyze the effect of this law on the leaching of rare earth ions.

2. Theory and Model

In the process of ionic rare earth in situ leaching, the leaching agent enters the interior of the ore body through the liquid injection hole and reacts with the rare earth ions adsorbed on the surface of the ore body to make them parse and leach out along with the seepage process [26, 27]. As shown in Figure 1, according to the ionic rare earth leaching kinetics of related research [28, 29], ionic rare earth leaching process, the leaching agent (taking magnesium sulphate solution as an example) first contacts with the liquid film layer on the surface of the rare earth ore particles. The magnesium ions in the leaching agent contact with the surface of the mineral particles through diffusion (liquid film diffusion) and then exchange with the rare earth ions on the surface of the ore body particles. After the ion exchange reaction between rare earth ions and magnesium ions, rare earth ions are resolved from the surface of the ore body, while magnesium ions are adsorbed to the particle surface of the ore body (ion exchange reaction). In the process of exchange reaction, magnesium ions can reach the surface of rare earth ion adsorption only through diffusion through the solid film layer of magnesium ion adsorption, and ion exchange reaction occurs with the adsorbed rare earth ions (solid film diffusion). The exchange rare earth ions enter the leaching agent by diffusion and exude the ore body with the leaching agent, so that the leaching process of rare earth ions is completed.

From this point of view, the efficient leaching of rare earth ions is not only related to the seepage of leaching agent and ion migration but also closely related to the ion exchange reaction on the particle surface of ore body. Therefore, the leaching process of rare earth ions can be regarded as a coupling process of seepage, exchange reaction, and ion migration.

2.1. Flow Control Equation. Assuming that the leaching agent is incompressible, its flow process in the pores of the ore body can be described by the Navier-Stokes equation [30], and the continuity equation is as follows:

$$\nabla \bullet u = 0, \tag{1}$$

where u is the velocity vector of the fluid (m/s). The equation of motion is as follows:

$$\rho\left[\frac{\partial u}{\partial t} + (u\bullet\nabla)u\right] = \nabla\bullet\left[-pI + \mu(\nabla u) + (\nabla u)^T\right] + F, \tag{2}$$

where p is fluid pressure (Pa); ρ is the fluid density (kg/m^3); μ is hydrodynamic viscosity; I is a unit tensor; t is time (s); and F is the volume force vector (N/m^3).

2.2. Ion Exchange Governing Equations. When the leaching agent flows in the pore, it also exchanges with rare earth ions adsorbed on the particle surface of the ore body [31]. It is assumed that rare earth ions adsorbed on the particle surface of the ore body transfer along the tangential direction of the surface, and this process can be described by Fick's law:

$$N_{t,i} = -D_{s,i}\nabla_t c_{s,i}, \tag{3}$$

where $N_{t,i}$ is the surface molar flux, mol/(m•s); $D_{s,i}$ is the

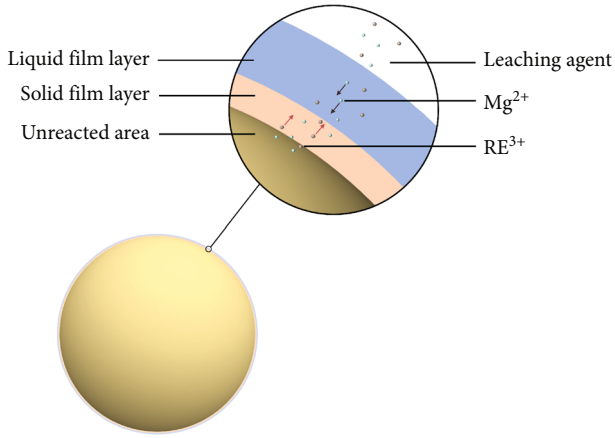

FIGURE 1: Schematic diagram of the rare earth ion exchange reaction.

surface diffusion coefficient of the substance i (m^2/s); and $c_{s,i}$ is the concentration of surface material i (mol/m^2). The governing equation of each substance concentration on the particle surface of the ore body is as follows:

$$\frac{\partial c_{s,i}}{\partial t} = -\nabla_t \bullet N_{t,i} + R_{s,i}, \tag{4}$$

where $R_{s,i}$ is the sum of source terms caused by surface reaction and adsorption analytical phenomenon ($mol/(m^2 \bullet s)$).

2.3. Solute Transport Governing Equation. After the exchange reaction, the rare earth ions enter the leaching agent and migrate in the ore body with the seepage process [32]. Considering convection and diffusion, the migration process of rare earth ions with leaching agent between pores of the ore body can be described by the convection-diffusion equation:

$$\frac{\partial c_i}{\partial t} + u \bullet \nabla c_i = R_i + \nabla \bullet D_i \nabla c_i, \tag{5}$$

where c_i is the concentration of substance i (mol/m^3); D_i is the diffusion coefficient of the substance i (m^2/s); R_i is the reaction rate of the substance i ($mol/(m^3 \bullet s)$); and u is the velocity vector of the fluid (m/s).

3. Model Establishment and Reliability Verification

3.1. Model Establishment. In the process of in situ leaching of ionic rare earth, the leaching agent fills the pores inside the ore body. The principle of magnetic resonance imaging is the resonance phenomenon of hydrogen protons under the action of strong magnetic field. The magnetic resonance imaging is obtained by data reconstruction of resonance trajectory data. In addition, the nuclear magnetic resonance test has the advantages of simple operation and accurate data, which provides convenience for the imaging of ion-type rare earth pore seepage channels in saturated state. The test samples on this paper were collected from an ionic rare earth mining area in Longnan County, Ganzhou City, Jiangxi Province. As shown in Figure 2, in order to obtain a more real internal pore structure of ionic rare earth ore body, in situ leaching stope, Luoyang shovel was used to dig to the bottom of the topsoil layer, a transparent acrylic pipe with a length of 300 mm and a diameter of 42 mm was driven into the ore body, and the tube body was drawn out to obtain a section of undisturbed ore body. A section of cylindrical sample with a height of 100 mm was intercepted, part of mineral soil at both ends of the sample was removed, and permeable stone was inserted to seal both ends of the sample. The samples were saturated with water for 48 h, so that the pores of the cylindrical sample will be filled with water. In order to eliminate the disturbance caused by sample interception and closed treatment, a nuclear magnetic resonance instrument (manufacturer: Suzhou Niumai Analytical Instrument Production Co., LTD., model: MesomR23-060H-I) was used to scan and image the 60 mm length of the sample in the middle of the sample in the axial direction. In the gray scale map of pore imaging generated, the higher the water content of ore samples, the stronger the NMR signal, and the brighter the pixels displayed in the image [33]. In order to reflect the characteristics of mineral soil aggregate structure, Mimics image control software was used to perform light source correction, image segmentation, filtering, and denoising on the image to digitize the solid phase skeleton and pore channels [34] and generate a two-dimensional geometric model of 42 mm × 60 mm (hereinafter referred to as the NMRI model).

The upper and lower boundaries of the model are inlet and outlet boundaries, respectively, and the left and right boundaries are flux-free boundaries. The wall of the seepage channel is the "surface region," and the leaching agent exchanges with the rare earth ion adsorbent on the "surface region." It is assumed that only the rare earth ions represented by yttrium (Y) element are uniformly distributed on the surface region, with a concentration of 0.12 mol/m^2. Studies on the leaching kinetics of in situ leaching show that [35, 36] mineral ion leaching is a process controlled by surface reaction, which is mainly affected by the exchange rate of leaching agent cation and mineral cation in leaching agent. In this study, magnesium sulphate solution is considered a leaching agent [37], and the chemical reaction equation between magnesium ion and rare earth ion can be expressed as follows:

$$\begin{aligned}&\left[Al_4(Si_4O_{10})(OH)_8\right]_m \cdot 2nRE^{3+}(s)\\ &\quad + 3nMg^{2+}(aq) \rightleftarrows \left[Al_4(Si_4O_{10})(OH)_8\right]_m \cdot 3nMg^{2+}(s)\\ &\quad + 2nRE^{3+}(aq)\end{aligned} \tag{6}$$

According to the above chemical reaction equation, the related exchange reaction rate, diffusion coefficient, and dispersion coefficient were calculated by the "reaction engineering" interface in COMSOL Multiphysics multiphysical coupling software. The model was imported into that software for coupling solution of the above governing equations.

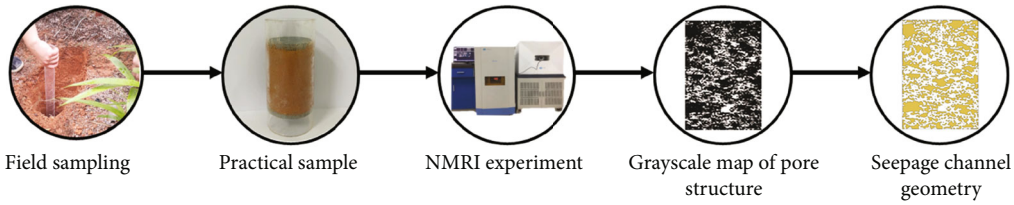

Figure 2: Construction steps of the NMRI model.

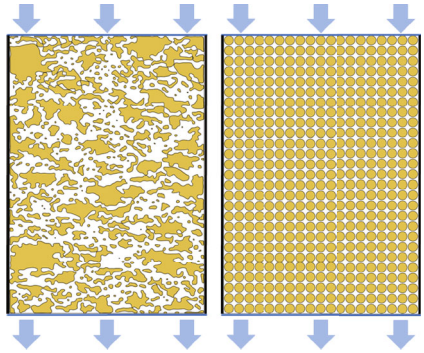

Figure 3: NMRI model and uniform model.

3.2. Test Method. In this study, the conditions of leaching agent concentration of 0.25 mol/L and injection strength of 1.0 mL/min were selected, and the uniform two-dimensional geometric model (hereinafter referred to as the uniform model) and the results of laboratory experiment were used for comparison with the NMRI model for validation.

As shown in Figure 3, it is assumed that the porosity of the uniform model is consistent with that of the unchanged ore sample measured in the laboratory test to be 0.37, and the particle diameter is 1.985 mm, and it is uniformly distributed in the model of 42 mm × 60 mm. The initial and boundary conditions are consistent with the NMRI model.

As shown in Figure 4, the ore sample selected for the indoor leaching test is the ore sample in the same interception section of nuclear magnetic imaging, and the leaching mother liquor is collected at the outlet end, and the content of rare earth ions in the mother liquor is measured by EDTA volumetric method (measured every 10 min and recorded) [38].

3.3. Verification of Simulation Results. Figure 5 shows the comparison between experimental results and simulation results of the average concentration of leached rare earth ions (hereinafter referred to as leaching concentration) changing with time under the condition of injection strength 1.0 mL/min and leaching agent concentration 0.25 mol/L. It can be seen from the figure that the change of leaching concentration over time in the NMRI model is similar to that in the laboratory test: the leaching agent has not reached the outlet at the initial stage of liquid injection, and the leaching concentration remains at a low level. When the leaching agent flows out from the outlet, the leaching concentration gradually reaches the peak, and the peak leaching concentrations under the NMRI model and the laboratory experiment are 9.1 g/L and 7.8 g/L, respectively. With the continuous infusion, the leaching concentration continued to decrease and gradually approached 0.0 g/L. At the same time, the decrease of rare earth ion concentration on the surface of ore body leads to the slowdown of chemical reaction rate, and the change rate of leaching rare earth ion concentration gradually decreases. According to the change of leaching concentration with time, the leaching process of the NMRI model and laboratory test can be divided into initial stage, ascending stage, peak stage, descending stage, and trailing stage. However, the variation of the average concentration of leached rare earth ions under the uniform model is quite different from that of the former two models. The difference is shown in the rising stage. The difference is shown in that the leaching concentration rises rapidly to the peak value of 13.1 g/L in a short time, during which there is a period of slow decline, and then enters a sharp descent process (the leaching concentration plummets to 0.0 g/L). The leaching process of the uniform model can be summarized as initial stage, ascending stage, peak stage, slow descent stage, and sharp descent stage.

Figure 6 shows the steady-state flow field cloud images of the uniform model and the NMRI model. In the uniform model, the distribution of the flow field around a single particle shows a certain regularity: the flow velocity on the left and right sides of the particle is larger, and the flow velocity at the smaller channel width is larger, and the maximum flow velocity can reach 6×10^{-5} m/s. The velocity at the upper and lower ends of the particle is very small, with the lowest velocity close to 0 m/s. The flow field in the NMRI model is more complex than that in the uniform model. On the whole, there is a dominant channel near the middle line in the vertical direction of the geometric model, which is divided into two tributaries from top to bottom. The flow velocity in the dominant channel area is larger than that in the nondominant channel area, and the maximum flow velocity can reach 6×10^{-4} m/s. The distribution of the flow field around a single particle is irregular, and the velocity at different locations is different.

Figure 7 shows the distribution cloud of rare earth ion concentration of the uniform model and the NMRI model at different times. In the uniform model, the particle size is small and the distribution is uniform, the leaching agent percolates uniformly downward in the pore, and the degree of rare earth ion exchange reaction is the same at the same level height, making the exchange reaction mainly concentrated in 25-170 min. However, the particle size and particle distribution of the NMRI model are nonuniform, and the flow field is more complex than that of the uniform model, which is similar to the seepage situation of ion-type rare earth minerals under real conditions. The exchange reaction in the

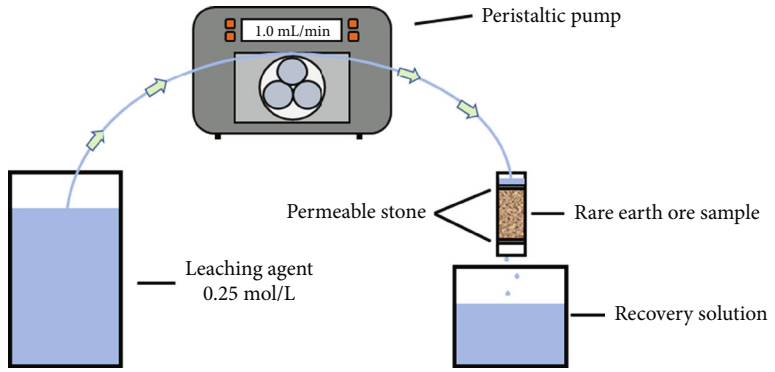

Figure 4: Schematic diagram of laboratory test.

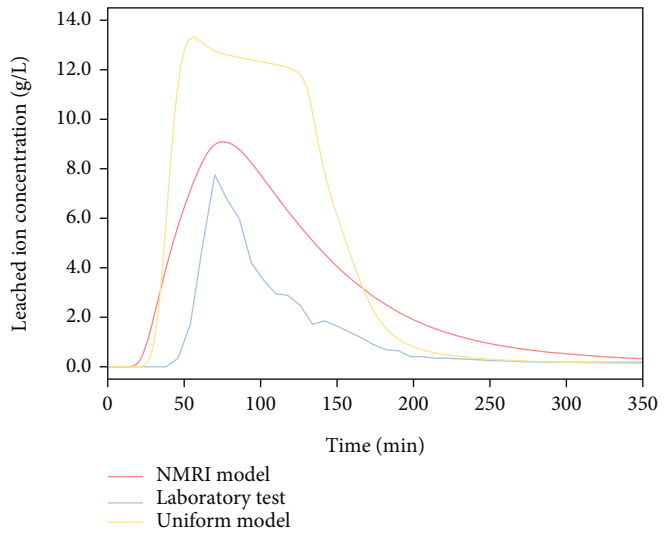

Figure 5: The comparison between the experimental value and the simulated value of the leaching concentration.

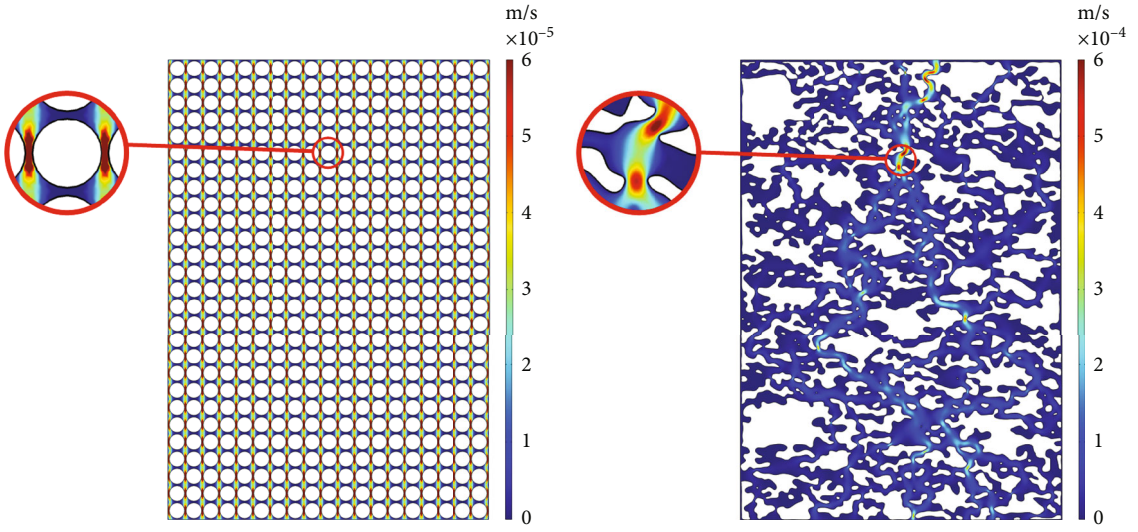

Figure 6: Steady-state flow field of the NMRI model and uniform model.

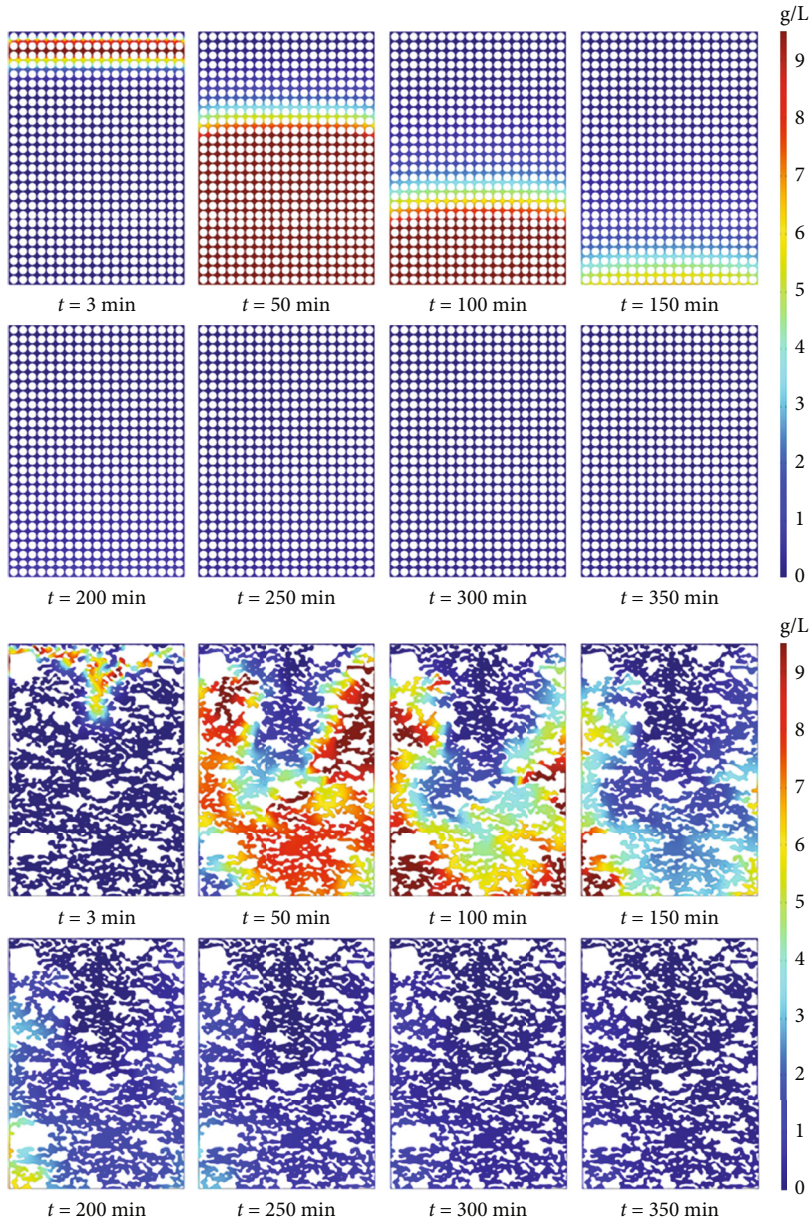

Figure 7: RE^{3+} ion migration processes in the NMRI model and uniform model.

dominant channel region occurred preferentially than that in the nondominant channel, and the exchange reaction lasted from 11 to 270 min. Therefore, the nonuniform model can reflect the exchange and migration of rare earth ions during in situ leaching to a certain extent.

4. Results and Discussion

4.1. Effect of Injection Strength on Leaching of Rare Earth Ions. In order to deeply understand the influence of the injection intensity on the leaching of rare earth ions, this study adopts the NMRI model and keeps the leaching agent concentration of 0.2 mol/L constant. The seepage-exchange-migration process of saturated leaching ore under different injection intensities (0.2 mL/min, 0.5 mL/min, 1.0 mL/min, and 2.0 mL/min) was studied.

Figure 8 shows the steady flow field cloud diagram under different injection intensities. With the increase of injection strength, the difference of flow velocity between dominant channel area and nondominant channel area is more obvious, and the maximum flow velocity is 1.3×10^{-4} m/s, 3.2×10^{-4} m/s, 6.5×10^{-4} m/s, and 1.3×10^{-3} m/s, respectively. As the flow rate in the dominant channel is greater than that in the nondominant channel, the leaching agent passing quantity in the dominant channel is greater than that in the nondominant channel in unit time. The flow velocity in the nondominant region is smaller than that in the dominant region, and increasing the injection intensity has limited effect on the flow velocity in the nondominant region, so the flow velocity change in this region is not obvious.

As shown in Figure 9, when the injection intensity is 0.2 mL/min, the peak leaching concentration is 8.9 g/L; when

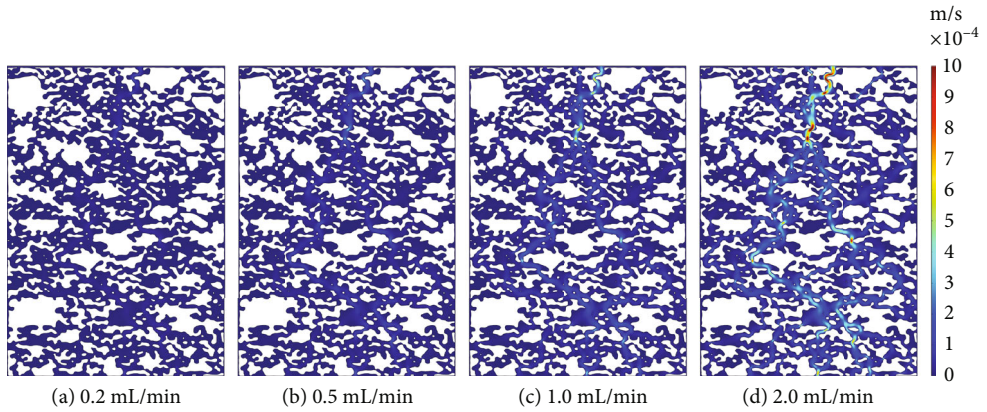

Figure 8: Steady-state flow field under different injection intensities.

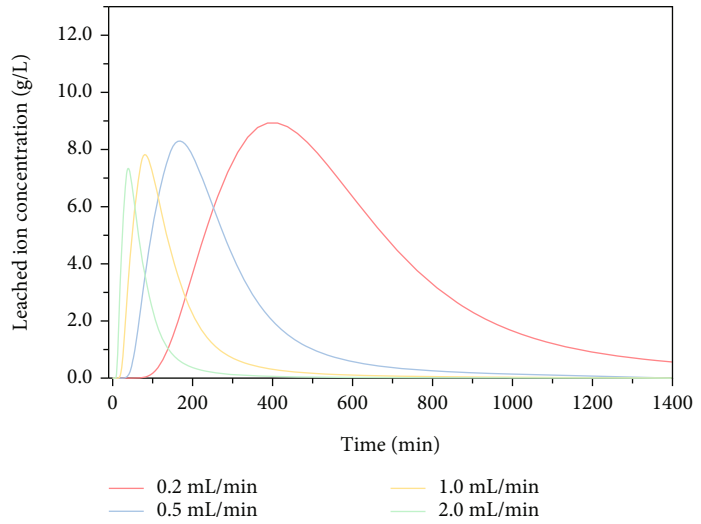

Figure 9: Variation curve of RE^{3+} ion leaching concentration under different injection intensities.

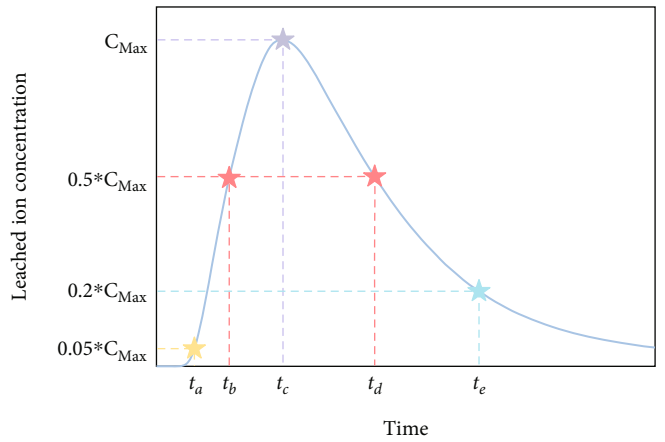

Figure 10: Schematic diagram of representative moments of rare earth ion leaching stage.

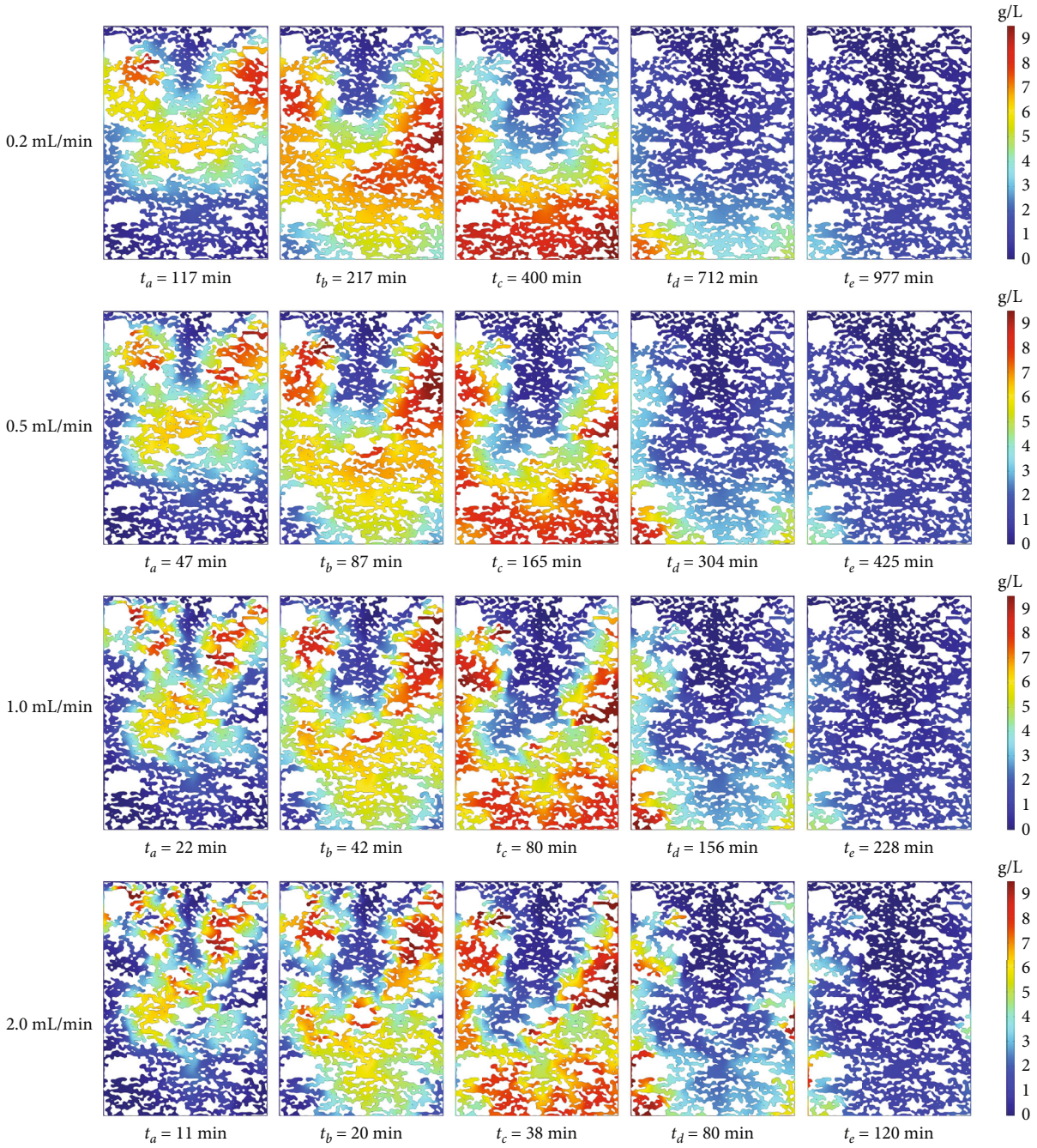

Figure 11: RE^{3+} ion migration process under different injection intensities.

the injection intensity increases to 0.5 mL/min, 1.0 mL/min, and 2.0 mL/min, the peak leaching concentration is 8.3 g/L, 7.8 g/L, and 7.3 g/L, respectively. This indicates that the peak concentration decreases with the increase of injection strength. At the same time, with the increase of liquid injection intensity, the corresponding time of peak concentration is $t = 400$ min, $t = 165$ min/$t = 80$ min, and $t = 38$ min, and the leaching concentration curve moves forward as a whole, indicating that increasing the liquid injection intensity can accelerate the whole leaching process to a certain extent, to shorten the leaching cycle.

Taking the time corresponding to the peak concentration of 5% in the initial stage, corresponding to the peak concentration of 50% in the rising stage, corresponding to the peak concentration in the peak stage, corresponding to the peak concentration of 50% in the falling stage, and corresponding to the peak concentration of 20% in the trailing stage as the representative times of the corresponding stages (as shown in Figure 10), Figure 11 shows the distribution cloud diagram of leached rare earth ion concentration at each stage under different injection intensities. In the initial stage, the exchange reactions are mainly concentrated in the

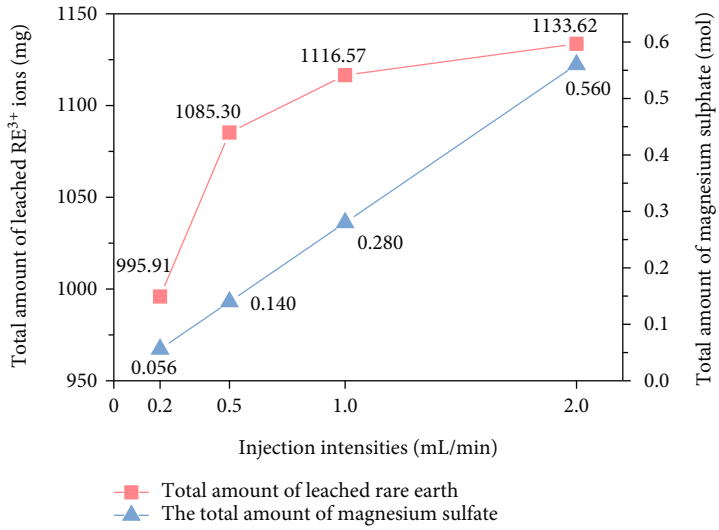

Figure 12: The total amount of leached RE^{3+} ions and the total amount of magnesium sulphate under different injection intensities.

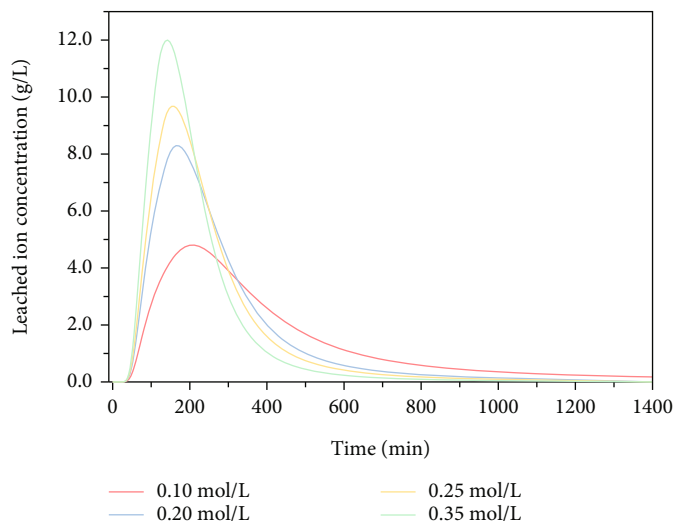

Figure 13: Variation curve of RE^{3+} ion leaching concentration with different leaching agent concentrations.

middle and upper part of the model. The surface reactions at the inlet end and the upper dominant channel are completed, and the rare earth ions migrate toward the outlet end with the leaching agent, so the concentration of rare earth ions there is low. In this stage, the replaced rare earth ions are mainly distributed in the upper nondominant channel and the middle dominant channel. The flow rate of the leaching agent in the nondominant channel is low, and the transport speed of leached rare earth ions in this region is less than that in the dominant channel, so the concentration of rare earth ions in the nondominant channel is higher at the same height at this stage. When the injection intensity increases, more leaching agents exchange reaction with the ore body in unit time, and the highest rare earth ion concentration in the upper nondominant channel also rises. Rising phase exchange reaction is mainly concentrated in the central model; the rare earth ions are mainly distributed in part of advantage channels and the upper advantage in the area; this phase is an obvious advantage bigger than the channel, and the rare earth ion migration velocity of nondominant channel, rare earth ions in the nondominant channel, and highest concentration increase with liquid injection strength and rise. The exchange reactions in the peak stage are mainly concentrated in the middle and lower part of the model, and the rare earth ions are mainly distributed in the lower dominant channel and the middle and lower nondominant channel regions. When the injection intensity increases, the highest leached rare earth concentration in the middle nondominant channel increases, while the rare earth ion concentration in the lower region decreases. This is also mutually verified with the phenomenon that the peak leaching concentration decreases with the increase of injection strength. The exchange reactions in the descending stage and trailing stage are mainly on the left and right sides of the lower part of the model, and rare earth ions are mainly distributed in the lower nondominant channel region. When

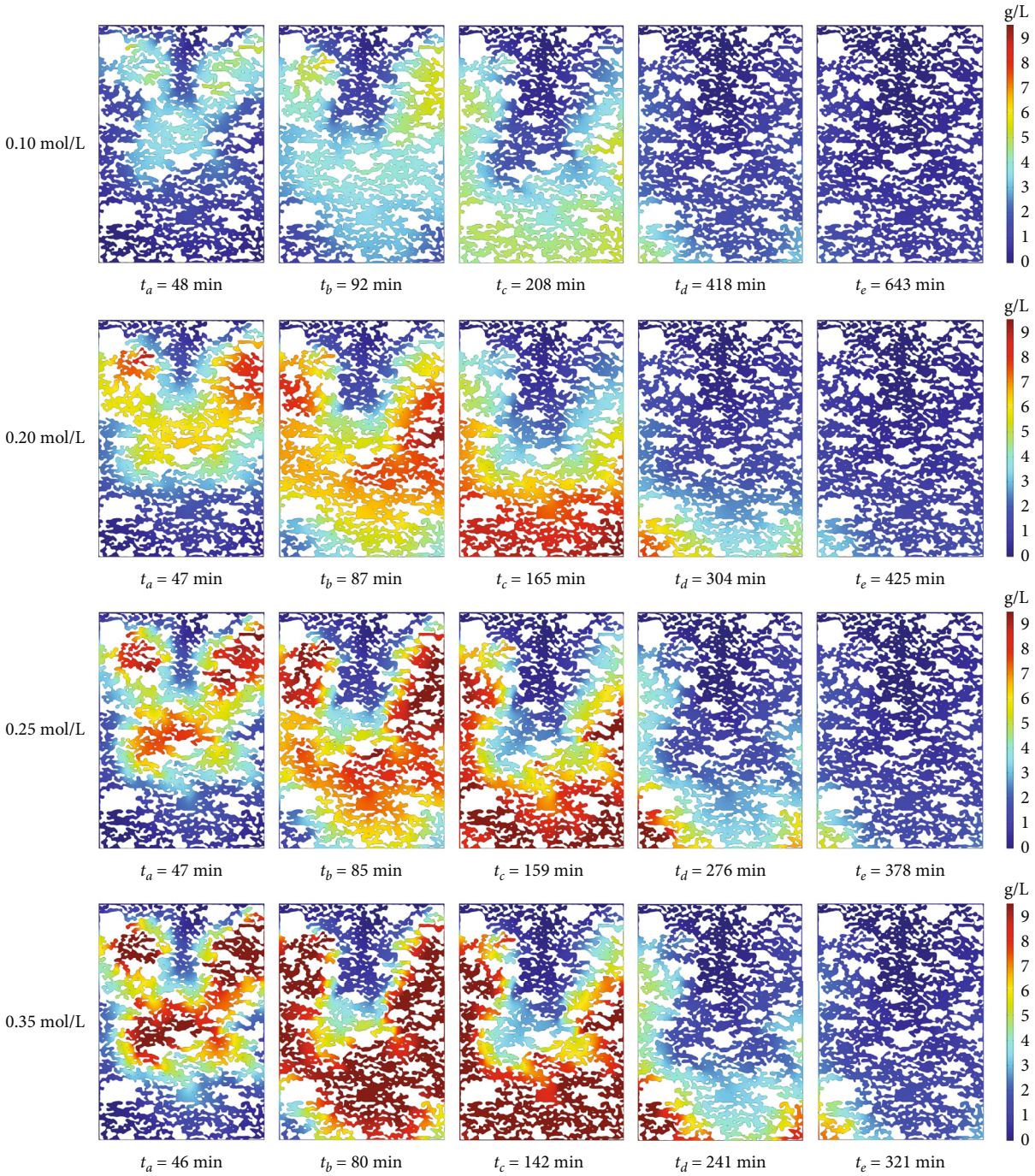

Figure 14: RE^{3+} ion migration process under different leaching agent concentrations.

the injection intensity increases, the overall concentration of rare earth ions in the middle and lower nondominant channel regions increases. It is obvious that the increase of injection intensity can promote the exchange reaction, and the rare earth ions in the nondominant channel region can be replaced more effectively. Convection in the dominant channel plays a dominant role in the migration of rare earth ions, while convection in the nondominant region has a relatively small effect on the migration of rare earth ions. Therefore, the migration velocity of rare earth ions in the dominant channel is greater than that in the nondominant region.

Figure 12 shows the total amount of leached rare earth ions and the total amount of magnesium sulphate under different injection strengths. It can be found from the figure that the total amount of magnesium sulphate (hereinafter referred to as the total amount) has a linear relationship with the intensity of the injection liquid, and the total amount of leached rare earth ions increases with the increase of the intensity of the injection liquid. Compared with 0.2 mL/min, the total dosage of 0.5 mL/min was increased by 150%, and the total amount of leached rare earth ions (hereinafter referred to as the total amount of leached) was

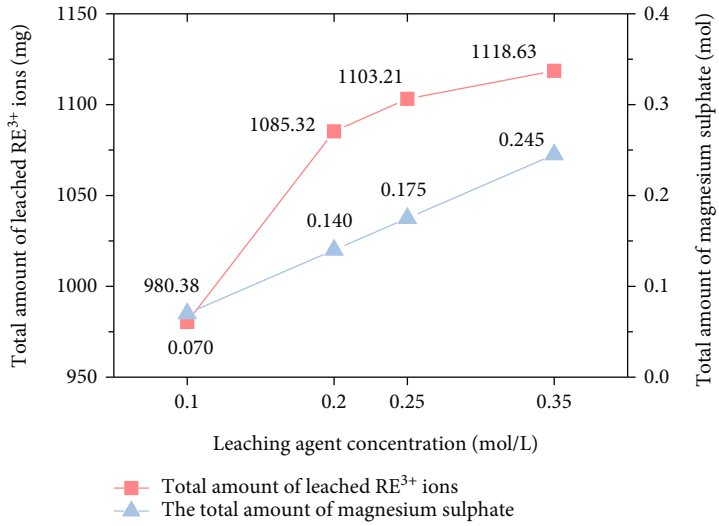

FIGURE 15: The total amount of leached RE^{3+} ions and the total amount of magnesium sulphate under different leaching agent concentrations.

increased by 8.9%; the total amount of 1.0 mL/min was increased by 100% compared with 0.5 mL/min, and the total amount of leaching was increased by 2.9%. Compared with 1.0 mL/min, the total dosage of 2.0 mL/min was increased by 100%, and the total leaching amount was increased by 1.5%. The increase of the total leaching amount decreased with the increase of the injection liquid intensity (i.e., the total dosage of magnesium sulphate). Combined with the analysis of the influence of liquid injection intensity on the flow velocity, it indicates that the limited effect of increasing liquid injection intensity on the flow velocity in the nondominant channel leads to the limited effect of increasing liquid injection intensity on the promotion of ion exchange reaction in the region.

Therefore, it is obvious that the influence of liquid injection intensity on leaching of rare earth ions is mainly reflected in the following aspects: with the increase of liquid injection intensity, the flow rate of all parts of the seepage channel increases accordingly, and more leaching agents enter the ore body and react with rare earth ions within a unit time, which accelerates the migration velocity of leaching rare earth ions and accelerates the whole leaching process. Moreover, the increase of the flow rate in the nondominant channel promotes the rare earth ion exchange reaction in this region. Due to the limitation of its promoting effect, the total amount of leached rare earth ions does not have a linear relationship with the injection intensity, but the growth rate decreases with the increase of the injection intensity. Based on the above analysis, after comprehensive consideration of factors such as leaching period, leached rare earth ion concentration, and total amount of magnesium sulphate, it is concluded that under this model, the injection intensity of 0.5~1.0 mL/min is more economical.

4.2. Influence of Leaching Agent Concentration on Rare Earth Ion Leaching. In order to deeply understand the influence of leaching agent on the leaching of rare earth ions, the NMRI model was used in this study. By controlling the injection strength of 0.5 mL/min, the seepage-exchange-migration process of saturated leaching under different leaching agents (0.10 mol/L, 0.20 mol/L, 0.25 mol/L, and 0.35 mol/L) was studied.

It is clear from Figure 13 that when the leaching agent concentration is 0.10 mol/L, the peak leaching concentration is 4.8 g/L, and when the injection intensity increases to 0.20 mol/L, 0.25 mol/L, and 0.35 mol/L, the peak leaching concentration is 8.3 g/L, 9.7 g/L, and 12.0 g/L, respectively. It indicates that the peak concentration increases with the increase of leaching agent concentration. Meanwhile, with the increase of leaching agent concentration, the corresponding time of peak concentration is $t = 208$ min, $t = 165$ min, $t = 159$ min, and $t = 142$ min, and the leaching concentration curves are basically in the same position, indicating that the acceleration effect of increasing leaching agent concentration on the whole leaching process is very limited, and the leaching cycle is basically unchanged.

The information given by Figure 14 is about the distribution cloud diagram of leaching rare earth ion concentration in each stage under different leaching agent concentrations. The representative time selected at the corresponding stage in the leaching process in the figure is as described in Section 4.1. On the whole, in the concentration of ore leaching reagents, the migration process of rare earth ions is roughly the same, and the main distribution area of rare earth ions is roughly the same as well. The difference is that the concentration of rare earth ions in the same distribution area in each stage increases with the increase of leaching agent, and the concentration of rare earth ions in the dominant channel and nondominant channel increases accordingly. This is because the increase of leaching agent concentration accelerates the exchange reaction rate, and more rare earth ions are leached per unit time, indicating that the increase of leaching agent concentration can promote the ion exchange reaction in all regions.

Figure 15 demonstrates the total amount of leached rare earth ions and the total amount of magnesium sulphate

under different leaching agent concentrations. As shown in the figure, the total dosage is linearly related to the injection strength, and the total amount of leached rare earth ions increases with the increase of the injection strength. The total amount of 0.20 mol/L increased by 100% compared with 0.10 mol/L, and the total amount of leaching increased by 10.7%. Compared with 0.20 mol/L, the total dosage of 0.25 mol/L increased by 25%, and the total leaching amount increased by 1.6%. Compared with the total dosage of 0.25 mol/L, 0.35 mol/L increased by 40%, and the total leaching amount increased by 1.4%. The increase of the total leaching amount decreased with the increase of leaching agent concentration (i.e., the total dosage of magnesium sulphate). Therefore, the promoting effect of leaching agent concentration on ion-exchange reaction in all regions is limited.

Therefore, the influence of leaching agent concentration on rare earth ion leaching is mainly reflected in when the concentration of leaching agent increases, the ion exchange reaction rate increases accordingly, and more rare earth ions are replaced into the leaching agent per unit time. However, the promoting effect of leaching agent concentration on ion exchange reaction is also limited. Based on the above analysis, after comprehensive consideration of factors such as leaching cycle, leaching rare earth ion concentration, and total magnesium sulphate consumption, it is concluded that under this model, the leaching agent concentration of 0.20~0.25 mol/L is more economical.

5. Conclusion

In this study, the three governing equations of solution seepage, ion exchange, and solute migration of ionic rare earth in situ leaching ore were used to construct a meso-ore body seepage channel model by using NMRI technology, and the reliability of the model was verified by indoor column leaching experiment. On this basis, the effects of injection strength and leaching agent concentration on the leaching of rare earth ions were discussed. The main conclusions are as follows:

(1) This model can simulate the internal seepage of ionic rare earth ore bodies at mesoscale. The internal seepage of ionic rare earth ore bodies at the mesoscale is more complex, and the flow field distribution is irregular, and there are dominant channels

(2) At the mesoscale, the ion exchange reaction in the dominant channel is completed preferentially than that in the nondominant channel region, and the migration of rare earth ions in the dominant channel with leaching agent is more affected by convection, and its migration velocity is greater than that in the nondominant channel region

(3) Increasing the injection strength and leaching agent concentration can promote the exchange and migration of rare earth ions. Based on the limitation of the promotion effect, the injection strength of 0.5~1.0 mL/min and the concentration of 0.20~0.25 mol/L leaching agent are considered to be more economical in practical engineering

Data Availability

The data that support the findings of this study are available from the corresponding author (VS) upon reasonable request.

Conflicts of Interest

The authors declare that there are no conflicts of interest regarding the publication of this paper.

Acknowledgments

This research was supported by the National Natural Science Foundation of China (51964014) and the Education Department of Jiangxi Province (GJJ209414).

References

[1] D. Wang, Y. Z. Rao, L. Shi, W. Xu, and T. Huang, "Relationship between permeability coefficient and fractal dimension of pore in ionic rare earth magnesium salt leaching ore," *Geofluids*, vol. 2022, Article ID 2794446, 13 pages, 2022.

[2] L. Liu, Y. Z. Rao, C. S. Tian et al., "Adsorption performance of La (III) and Y (III) on orange peel: impact of experimental variables, isotherms, and kinetics," *Adsorption Science & Technology*, vol. 2021, article 7189639, 12 pages, 2021.

[3] B. Fan, L. S. Zhao, Z. Y. Feng et al., "Leaching behaviors of calcium and magnesium in ion-adsorption rare earth tailings with magnesium sulfate," *Transactions of Nonferrous Metals Society of China*, vol. 31, no. 1, pp. 288–296, 2021.

[4] Z. Q. Guo, J. F. Jin, K. Zhao, X. J. Wang, and G. L. Chen, "Status of leaching technology and theory of ion adsorption type rare earth ores," *Chinese Rare Earths*, vol. 2018, no. 1, pp. 132–141, 2018.

[5] Z. X. Tang, M. N. Li, and D. Yang, "Application and prospect of in-situ leaching mining method in ionic rare earth ores," *Hunan Nonferrous Metals*, vol. 1998, no. 4, p. 3, 1998.

[6] L. Tao, A. X. Wu, Y. T. Feng et al., "Coupled DEM-LBM simulation of saturated flow velocity characteristics in column leaching," *Minerals Engineering*, vol. 128, pp. 36–44, 2018.

[7] S. H. Luo, T. Luo, G. S. Wang, J. Liu, S. Hu, and D. Zhu, "Effect of heterogeneity of leaching solution on leaching rate in ionic rare earth ore body," *The Soil*, vol. 50, no. 2, pp. 421–427, 2018.

[8] L. Shi, Y. Z. Rao, D. Wang, M. D. Zhang, and T. Huang, "A capillary model for predicting saturated hydraulic conductivity of ion-adsorption rare earth ore based on improved Kozeny–Carman equation," *Geofluids*, vol. 2022, Article ID 2947220, 10 pages, 2022.

[9] R. W. Bartlett, "Simulation of ore heap leaching using deterministic models," *Hydrometallurgy*, vol. 29, no. 1–3, pp. 231–260, 1992.

[10] A. X. Wu, J. Z. Liu, S. H. Yin, and X. Yong, "The mathematical model of the solute transportation in the heap leaching and the analytic solutions," *Mining and Metallurgical Engineering*, vol. 25, no. 5, pp. 7–10, 2005.

[11] C. Y. Wu, Y. S. Qiu, and L. M. Wang, "Numerical study on solute transport in leaching process of rare earth by lattice

Boltzmann method," *The Chinese Journal of Process Engineering*, vol. 14, no. 5, pp. 730–736, 2014.

[12] G. A. Sheikhzadeh, M. A. Mehrabian, S. H. Mansouri, and A. Sarrafi, "Computational modelling of the unsaturated flow of liquid in heap leaching, using the results of column tests to calibrate the model," *International Journal of Heat and Mass Transfer*, vol. 218, no. 4, pp. 277–289, 2004.

[13] J. Z. Liu, B. H. Yang, and Y. H. Li, "Coupling mechanism and numerical simulation analysis of leaching process," *Mining and Metallurgical Engineering*, vol. 35, no. 2, pp. 114–116, 2015.

[14] S. L. Hu, X. J. Cao, G. S. Wang, P. Long, and X. Y. Zhou, "Ion exchange model for leaching process of weathered crust leaching rare earth ore," *Mining and Metallurgical Engineering*, vol. 38, no. 4, pp. 1–5, 2018.

[15] P. Long, G. S. Wang, J. Tian, S. L. Hu, and S. H. Luo, "Simulation of one-dimensional column leaching of weathered crust elution-deposited rare earth ore," *Transactions of Nonferrous Metals Society of China*, vol. 29, no. 3, pp. 625–633, 2019.

[16] A. X. Wu, J. Z. Liu, and L. Y. Tang, "Simulation of coupled flowing-reaction-deformation with mass transfer in heap leaching processes," *Applied Mathematics and Mechanics*, vol. 28, no. 3, pp. 327–335, 2007.

[17] A. X. Wu, S. H. Yin, H. J. Wang, and Y. D. Su, "Mechanism and model of solute transport in heap leaching process," *Journal of Central South University (Science and Technology)*, vol. 37, no. 2, pp. 385–389, 2006.

[18] C. L. Tan, *Research on seepage-reaction-stress coupling in the leaching process of ion-type rare earth ore*, Jiangxi University of Science and Technology, Ganzhou, 2021.

[19] D. Ma, H. Y. Duan, and J. X. Zhang, "Solid grain migration on hydraulic properties of fault rocks in underground mining tunnel: radial seepage experiments and verification of permeability prediction," *Tunnelling and Underground Space Technology*, vol. 126, article 104525, p. 14, 2022.

[20] D. Ma, H. Y. Duan, J. X. Zhang et al., "Numerical simulation of water–silt inrush hazard of fault rock: a three-phase flow model," *Rock Mechanics and Rock Engineering*, vol. 55, no. 8, pp. 5163–5182, 2022.

[21] Q. Li, D. Ma, Y. D. Zhang, Y. Liu, and Y. J. Ma, "Insights into controlling factors of pore structure and hydraulic properties of broken rock mass in a geothermal reservoir," *Lithosphere*, vol. 2022, article 3887832, 17 pages, 2022.

[22] B. H. Yang, A. X. Wu, X. X. Miao, and J. Z. Liu, "3D characterization and analysis of pore structure of packed ore particle beds based on computed tomography images," *International Journal of Mining Science and Technology*, vol. 24, no. 3, pp. 833–838, 2014.

[23] A. X. Wu, B. H. Yang, J. Z. Liu, and J. Zhang, "Analysis of pore evolution law during leaching process of ore bulk based on X-ray CT technology," *The Chinese Journal of Process Engineering*, vol. 7, no. 5, pp. 960–966, 2007.

[24] X. P. Luo, Y. B. Zhang, H. P. Zhou et al., "Pore structure characterization and seepage analysis of ionic rare earth orebodies based on computed tomography images," *International Journal of Mining Science and Technology*, vol. 32, no. 2, pp. 411–421, 2022.

[25] C. G. Huang, *Experimental study on the influence of ionic strength and pH of leaching solution on the leaching effect of ionic rare earths*, Jiangxi University of Science and Technology, Ganzhou, 2021.

[26] C. F. Liu, F. Zhou, X. Y. Wu, J. Feng, and R. A. Chi, "Research status and prospect of leaching, seepage and mass transfer process of weathered crust leaching rare earth ores," *Chinese Rare Earths*, vol. 42, no. 1, pp. 111–121, 2021.

[27] R. A. Chi and X. M. Liu, "Current situation and prospects of exploitation of weathered crust leach-accumulated rare earth ores," *Journal of the Chinese Society of Rare Earths*, vol. 37, no. 2, pp. 129–140, 2019.

[28] Y. T. Li, A. B. Tu, Y. F. Zhang, M. Zhang, and R. A. Chi, "Kinetics of leaching rare earth from a weathered crust elution–deposited rare earth ore in South China with mixed ammonium salt," *Industrial Minerals & Processing*, vol. 38, no. 2, pp. 19–24, 2009.

[29] Z. Chen, Z. Y. Zhang, N. J. Sun, H. Zhang, Z. Liu, and R. A. Chi, "Leaching kinetics of weathered crust elution-deposited rare earth ore with magnesium salt," *Metal Mine*, vol. 2018, no. 8, pp. 84–91, 2018.

[30] M. Panah and F. Blanchette, "Simulating flow over and through porous media with application to erosion of particulate deposits," *Computers & Fluids*, vol. 166, pp. 9–23, 2018.

[31] Z. Q. Guo, K. Zhao, J. F. Jin, Z. C. Zhu, and G. Li, "Solute transport mechanism of ion-adsorption type rare earth in- situ leaching mining," *Journal of the Chinese Society of Rare Earths*, vol. 37, no. 1, pp. 121–128, 2019.

[32] J. Liu and B. H. Brady, "Evaluation of velocity-dependent in situ leaching processes: single-porosity model," *Metallurgical and Materials Transactions*, vol. 29, no. 6, pp. 1227–1234, 1998.

[33] K. P. Zhou, J. L. Li, Y. J. Xu, and Y. M. Zhang, "Measurement of rock pore structure based on NMR technology," *Journal of Central South University (Science and Technology)*, vol. 43, no. 12, pp. 4796–4800, 2012.

[34] L. M. Hu, D. T. Lin, P. W. Zhang et al., "Pore structure model for media and application in seepage analysis," *Journal of Taiyuan University of Technology*, vol. 53, no. 3, pp. 360–370, 2022.

[35] X. W. Chai, G. Q. Li, Z. Y. Zhang, R. Chi, and Z. Chen, "Leaching kinetics of weathered crust elution-deposited rare earth ore with compound ammonium carboxylate," *Minerals*, vol. 10, no. 6, p. 516, 2020.

[36] J. Tian, X. K. Tang, J. Q. Yin, and X. P. Luo, "Present situation of fundamental theoretical research on leaching process of weathered crust elution-deposited rare earth ore," *Nonferrous Metals Science and Engineering*, vol. 3, no. 4, pp. 48–52, 2012.

[37] Y. F. Xiao, Y. Y. Chen, Z. Y. Feng et al., "Leaching characteristics of ion-adsorption type rare earths ore with magnesium sulfate," *Transactions of Nonferrous Metals Society of China*, vol. 25, no. 11, pp. 3784–3790, 2015.

[38] L. H. Gao, R. R. Xing, Y. R. Zhu, and W. Y. Zhao, "Total amount of rare earth in rare earth ferroalloy was determined by EDTA titration," *Metallic Functional Materials*, vol. 29, no. 4, pp. 98–102, 2022.